

Review



Cite this article: Kralchevsky PA, Danov KD, Petkov PV. 2016 Soft electrostatic repulsion in particle monolayers at liquid interfaces: surface pressure and effect of aggregation. *Phil. Trans. R. Soc. A* **374**: 20150130. <http://dx.doi.org/10.1098/rsta.2015.0130>

Accepted: 2 December 2015

One contribution of 15 to a discussion meeting issue 'Soft interfacial materials: from fundamentals to formulation'.

Subject Areas:

chemical physics, physical chemistry

Keywords:

particle monolayers, charged colloids, surface pressure, limited aggregation

Author for correspondence:

Peter A. Kralchevsky
e-mail: pk@lcpe.uni-sofia.bg

Soft electrostatic repulsion in particle monolayers at liquid interfaces: surface pressure and effect of aggregation

Peter A. Kralchevsky, Krassimir D. Danov and

Plamen V. Petkov

Department of Chemical and Pharmaceutical Engineering, Faculty of Chemistry and Pharmacy, Sofia University, Sofia 1164, Bulgaria

 PAK, 0000-0003-3942-1411

Non-densely packed interfacial monolayers from charged micrometre-sized colloid particles find applications for producing micropatterned surfaces. The soft electrostatic repulsion between the particles in a monolayer on an air/water (or oil/water) interface is mediated by the non-polar fluid, where Debye screening is absent and the distances between the particles are considerably greater than their diameters. Surface pressure versus area isotherms were measured at the air/water interface. The experiments show that asymptotically the surface pressure is inversely proportional to the third power of the interparticle distance. A theoretical model is developed that predicts not only the aforementioned asymptotic law but also the whole surface pressure versus area dependence. An increase in the surface pressure upon aggregation of charged particles in the interfacial monolayers is experimentally established. This effect is explained by the developed theoretical model, which predicts that the surface pressure should linearly increase with the square root of the particle mean aggregation number. The effect of added electrolyte on the aggregation is also investigated. The data lead to the conclusion that 'limited aggregation' exists in the monolayers of charged particles. In brief, the stronger electrostatic repulsion between the bigger aggregates leads to a higher barrier to their coalescence that, in turn, prevents any further aggregation, i.e. negative feedback is present.

This article is part of the themed issue 'Soft interfacial materials: from fundamentals to formulation'.

1. Introduction

Electrically charged micrometre-sized particles on a liquid (air/water or oil/water) interface form a monolayer of a regular hexagonal lattice with interparticle distances that are significantly larger than both the particle diameter and the Debye screening length in the aqueous phase [1–5]. The long-range interparticle repulsion in such monolayers is due to the electrostatic field created by the particles in the *non-polar* fluid (air, oil) [4,6]. The non-densely packed colloidal layers that are formed have been investigated in relation to their potential use for producing micropatterned surfaces with applications for superhydrophobic and anti-reflection coatings [7–9], microlens arrays [10,11] and structures for bioengineering and biosensing [12,13]. The properties of the non-densely packed colloidal layers are also important for phase-transfer catalysis [14,15], the stability of Pickering emulsions [16–19] and for modelling the interactions in monolayers of charged macromolecules (e.g. globular proteins) [20] and nanoparticles [21]. The surface pressure of monolayers from charged particles and particle aggregation in such monolayers was first studied in [4,5]. Their dilatational elasticity has also been investigated [21].

To elucidate the main difference between monolayers of surfactant molecules and charged particles, let us consider the two-dimensional van der Waals equation, which is frequently used to describe the surface pressure, Π , of adsorption monolayers [22],

$$\Pi = \frac{\Gamma kT}{1 - \Gamma/\Gamma_\infty} - \beta\Gamma^2. \quad (1.1)$$

Here, Γ is the number of molecules (particles) per unit area; Γ_∞ is the limiting value of Γ at close packing; k is the Boltzmann constant; T is the absolute temperature; and β is a constant interaction parameter, which is positive (negative) for attractive (repulsive) interactions between the adsorbed molecules. The first term on the right-hand side of equation (1.1) expresses the contribution due to entropy (thermal motion of adsorbed molecules), which accounts for the excluded-area effect. In the case of surfactant monolayers, using typical parameter values, $1/\Gamma = 0.60 \text{ nm}^2$ and $1/\Gamma_\infty = 0.30 \text{ nm}^2$, we find that the entropy term in equation (1.1) is 13.7 mN m^{-1} and it dominates the surface pressure, Π . By contrast, taking the typical values for a monolayer of micrometre-sized particles, $1/\Gamma = 12 \text{ }\mu\text{m}^2$ and $1/\Gamma_\infty = 6 \text{ }\mu\text{m}^2$, we estimate that the entropy term in equation (1.1) is only $6.8 \times 10^{-7} \text{ mN m}^{-1}$. The latter value is absolutely negligible when compared with the experimental Π , which can be up to 50 mN m^{-1} [4,5]. In other words, for monolayers of micrometre-sized charged particles the entropy contribution to the surface pressure Π is completely negligible. In such a case, Π is dominated by the soft- and long-range repulsion between the charged particles.

Because $\Gamma = 1/\alpha$, where α is the mean area per particle in the monolayer, the interaction term in equation (1.1) is $\Pi \approx \beta\Gamma^2 \propto 1/\alpha^2 \propto 1/L^4$, where L is the mean distance between two neighbouring particles. However, the experiment indicates that the asymptotic behaviour of the surface pressure at large interparticle distances is $\Pi \propto 1/L^3$ [23], i.e. it has a longer range than predicted by the van der Waals equation.

One of our goals in this article is the explanation of the dependence of surface pressure Π on the interparticle distance L . The paper represents a brief review of our recent results [23,24], as well as related results from other studies, and considers also the effects of particle aggregation and added electrolyte on the surface pressure of monolayers from charged particles. The experimental system and results are described in §2. Theoretical models are presented and compared with experimental data in §3. Conclusions are presented and possible future developments are discussed in §4.

2. Experimental system and results

(a) Material and methods

The silica particles, Excelica UF305 (Tokuyama Corp., Japan), were produced by melting synthetic SiO_2 . The particles are spherical, but polydisperse. They have a lognormal size distribution with a

maximum corresponding to the particle radius, $R_p = 1.92 \mu\text{m}$. The radii of 50% of the particles are in the range $1.56 \leq R_p \leq 2.37 \mu\text{m}$. The procedure for particle cleaning and hydrophobization by dichlorodimethylsilane (DCDMS, 99.5%; Fluka) is described elsewhere [23,24]. The contact angle of the hydrophobized particles, $\theta = 94^\circ \pm 2^\circ$ [24], was measured by side-view observations, as in [4]. Insofar as the boundary between hydrophilicity and hydrophobicity is at $\theta = 90^\circ$, our particles with $\theta = 94^\circ$ are weakly hydrophobic.

After their hydrophobization, the particles were stored in a sealed beaker with 20 ml isopropyl alcohol (IPA). At the beginning of each experiment, a sample of the particle suspension in IPA was taken with a pipette and spread on the surface of water in a Langmuir trough (KSV NIMA Minimicro trough). The IPA evaporated and a particle monolayer was deposited on the water surface. The surface pressure Π was measured by using a Wilhelmy plate made of filter paper. All experiments were carried out at a temperature of 25°C .

The particle monolayers formed in the trough were observed from below by means of an inverted microscope (Axiovert 40 MAT; Carl Zeiss). The inner dimensions of the trough were $195 \times 51 \times 4 \text{ mm}$. The trough was filled with an aqueous phase of volume 30 ml (thickness 3 mm). After placing several (six to eight) drops of the particle suspension in IPA on the water surface between the barriers, we waited for 1–2 h until a stable constant value of Π was established. The surface area between the barriers varied from 85.6 to 14.4 cm^2 , and vice versa in each cycle of the monolayer compression and subsequent expansion at a constant surface rate of $5.1 \text{ cm}^2 \text{ min}^{-1}$. The compression and the subsequent expansion were separated by an interval of 100 s to allow relaxation of the monolayer.

By placing a needle-shaped electrode (tip curvature radius $147 \mu\text{m}$) in the air at 1.5 mm above the monolayer, we established that the particles are negatively charged. In this experiment, for potentials 0, +500 and +2400 V on the electrode (relative to ground) we determined the mean area per particle, respectively, as 110, 105 and $75 \mu\text{m}^2$ in the region below the electrode. By contrast, for potentials -500 and -2400 V large domains that are free of particles were observed just below the electrode. In other words, the particles are attracted by a positively charged electrode and repelled by a negatively charged one. Thus, we can conclude that the charges, which create the particle electric field in the air, are negative. A detailed theoretical description of the interaction of charged colloid particles at air/water and oil/water interfaces with an external electric field in the non-polar fluid (air, oil) can be found in [25].

The interparticle distances in the monolayer at a given degree of compression indicate that the surface charge acquired by the particles in different hydrophobization runs is not perfectly reproducible, despite the fact that we are following exactly the same experimental procedure. For this reason, in a given series of experiments with the Langmuir trough, we used particles from the *same* batch for a period of less than one week. For longer storage in IPA, a pronounced decrease of the particle charge is observed. For example, after particle storage in IPA for 1, 13 and 17 days, we determined that the particle surface charge density, respectively, was $\sigma = 0.21, 0.14$ and $0.12 \mu\text{C cm}^{-2}$ (see [23] for details). The decrease in σ during storage in IPA could be explained by the desorption of ions bound to the particle surfaces, which is facilitated by the relatively high dielectric constant of IPA, $\varepsilon = 18.6$ at 25°C .

Frames from video recordings corresponding to different degrees of compression (i.e. to different area, A , between the barriers) were processed and the mean area per particle in the monolayer, α , was determined. A and α are related by the simple formula $A = N\alpha$, where N is the total number of particles between the barriers in the trough. The experimental plot of A versus α is a linear dependence, which means that there is no loss of particles during the compression due, for example, to particle detachment from the interface and sinking in the subphase. From the slope of this dependence, we can determine N (see [23,24] for details).

In addition, to characterize the surface charge at the particle/water interface, the particle ζ -potential was measured as a function of the electrolyte concentration in the aqueous phase. Negative ζ -potentials have been measured. The maximal magnitude of the ζ -potential, -76 mV , was registered at a concentration of 1 mM added KCl [24]. The ζ -potentials were measured with particles hydrophobized as explained above. After storing the particles in IPA,

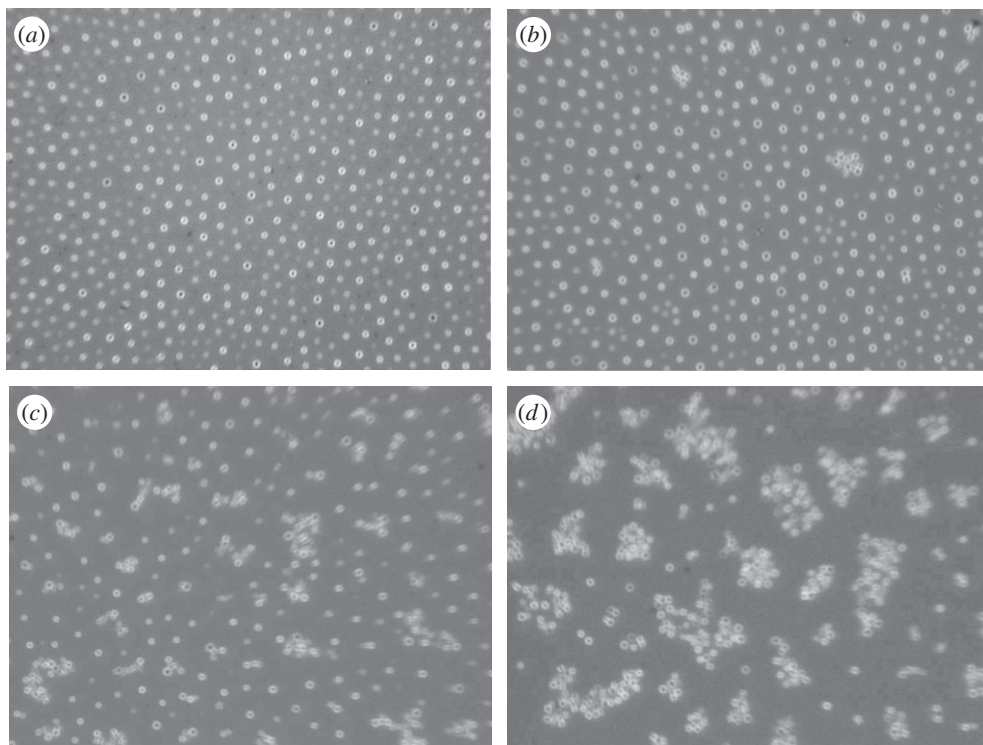


Figure 1. Monolayers from charged hydrophobized silica particles (of mean radius $R_p = 1.9 \mu\text{m}$) at the air/water interface in a Langmuir trough. (a) A compressed particle monolayer on the surface of the water (no added electrolyte). (b) After the first compression/expansion cycle, the formation of small aggregates is observed. On the surface of aqueous electrolyte solutions, stronger particle aggregation is observed: (c) 0.1 mM KCl; (d) 1 mM KCl. The photos show domains of size $289 \times 217 \mu\text{m}$.

the obtained suspension was sonicated; 45 min later, the large particles sedimented, whereas the fraction of small particles, of diameters $0.8\text{--}0.9 \mu\text{m}$, remained dispersed in IPA. The ζ -potential measurements were carried out with the latter fraction of small particles. By contrast, the experiments with the Langmuir trough were carried out with the fraction of the larger (sedimented) particles of average diameter $3.84 \mu\text{m}$.

(b) Experimental results

Figure 1*a* shows a typical photograph of the particle monolayer. Even in a relatively compressed state, no pronounced particle aggregation is observed. However, after a cycle of compression and expansion, the formation of separate small aggregates in the monolayer can be seen (figure 1*b*). The empty area around these aggregates is markedly larger than that around the single particles, which indicates that the aggregates strongly repel the surrounding particles. As illustrated in figure 1*c,d*, the addition of electrolyte (KCl) in the aqueous phase causes aggregation that increases with as the electrolyte concentration increases.

The surface-pressure isotherms in figure 2 represent illustrative data from experiments with two batches of particles: experiment 1 with a higher particle charge and experiment 2 with a lower particle charge.

Figure 2*a* (experiment 1) shows that, after each compression/expansion cycle, the surface pressure Π increases. Figure 2*b* shows the same data, but plotted as Π versus $A^{-3/2}$. It can be seen that the data are linear, in agreement with the experimental findings in [23] for monolayers

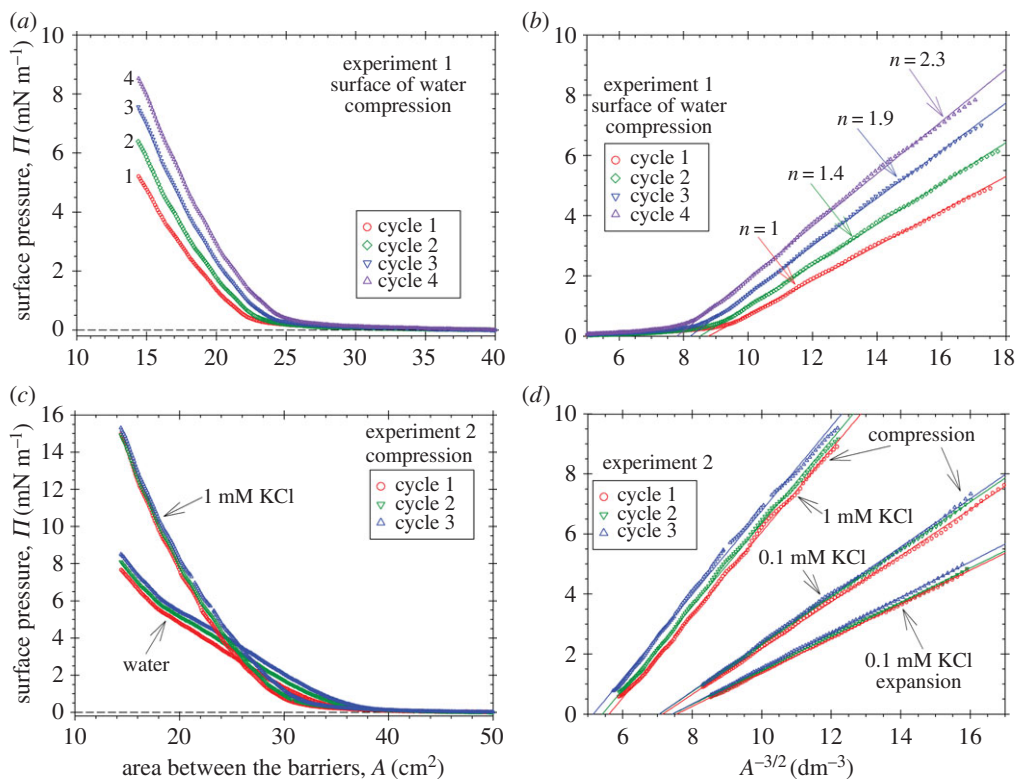


Figure 2. Surface pressure, Π , of monolayers from charged hydrophobized silica particles at the air/water interface measured by a Langmuir trough. (a) Plots of Π versus the area, A , for four consecutive compression/expansion cycles with the same monolayer on the surface of pure water. (b) The same data are plotted as Π versus $A^{-3/2}$; from the slopes of the linear portions the values of the mean particle aggregation number, n , can be determined, as shown in the figure. (c) Comparison of Π versus A isotherms for particle monolayers at the surface of pure water and an aqueous solution of 1 mM KCl. (d) Comparison of Π versus $A^{-3/2}$ plots for particle monolayers on the surface of a 0.1 mM KCl solution (compression and expansion) and a 1 mM KCl solution (compression). (After [24].)

of charged particles at both air/water and oil/water interfaces. The linear portions of the curves obey the equation

$$\Pi = CA^{-3/2} + \Pi_0, \quad (2.1)$$

where the coefficient C characterizes the slope of the experimental line and Π_0 is a background surface pressure. The slanted parts of the $\Pi(A)$ isotherms (figure 2a–c), corresponding to higher A (and lower Π) values, can be explained by the fact that the electrostatic interaction has a certain range, so that above a given distance between the particles they are not strongly interacting and, thus, only a ‘gas’ phase of particles is present. Our study is focused on the steep parts of the surface-pressure isotherms, corresponding to the compression of particle monolayers without voids. Note that equation (2.1) is obeyed by monolayers from monodisperse particles, as well as by monolayers from slightly polydisperse particles such as those used in this study [23].

Figure 2c (experiment 2) compares $\Pi(A)$ isotherms measured with the same amount of particles, from the same batch, but spread on the surface of a water and 1 mM KCl solution. The data indicate that at the smaller values of A (at the higher degrees of compression) Π is higher for the monolayer spread on the surface of the 1 mM KCl solution. This result seems paradoxical, because the electrolyte is expected to suppress the electrostatic interparticle repulsion and to lower the surface pressure Π . A possible explanation for this result is proposed in §3d.

Figure 2d illustrates three experimental facts, namely (i) the experimental curves possess large linear portions when plotted as Π versus $A^{-3/2}$; (ii) the magnitude of the surface pressure Π

increases with increasing KCl concentration; and (iii) for the same KCl concentration (0.1 mM), Π is systematically lower on expansion than on compression, i.e. a pronounced hysteresis effect is present. Moreover, the curves in figure 2c,d indicate good reproducibility of the experimental curves obtained in three consecutive compression/expansion cycles. The theory of the surface pressure of monolayers from charged particles is presented in the next section and possible explanations for the observed effects are proposed.

3. Theory of the surface pressure of monolayers from charged particles

(a) Force of electrostatic repulsion between two floating particles

Here, we consider electrically charged spherical dielectric particles attached to the interface between a water phase of dielectric constant ε_w and a non-polar fluid (air, oil) of dielectric constant ε_n . As already mentioned, if the particle radius, R_p , and the centre-to-centre distance between two particles, L , are of the order of micrometres, i.e. much greater than the Debye screening length in the aqueous phase, κ^{-1} , the interparticle repulsion is mediated by the electric field in the non-polar fluid. Theoretical investigations have shown that in such a case the electric field created by each particle in the non-polar fluid has a dipolar character, as shown in figure 3a. Asymptotically, the electric field of each particle is equivalent to the field of a dipole of effective dipole moment p_d , which is oriented perpendicular to the liquid interface. The force of electrostatic repulsion between two such dipoles is [4,26,27]

$$F_{ER} = \frac{3p_d^2}{2\varepsilon_n L^4} \quad (L \gg r_c, \kappa^{-1}). \quad (3.1)$$

The factor 2 in the denominator of equation (3.1) accounts for the fact that the dipolar field occupies only the upper half-space (the non-polar fluid), whereas the electric field in the aqueous phase is screened by the ions in water; r_c is the contact-line radius.

In the case of an electric field created by charges at the *particle/non-polar fluid* interface (figure 3b), the electrostatic boundary problem has been solved in bispherical coordinates using the Mehler–Fock integral transform and the following expression for p_d has been derived [28]:

$$p_d = 4\pi\sigma D(\theta, \varepsilon_{pn}) R_p^3 \sin^3 \theta. \quad (3.2)$$

Here, θ is the contact angle (figure 3b); σ is the electric charge density at the particle/non-polar fluid interface; $D = D(\theta, \varepsilon_{pn})$ is a known dimensionless function, which can be calculated by means of table 1 and eqn (D.1) in [28]; and $\varepsilon_{pn} \equiv \varepsilon_p/\varepsilon_n$ is the ratio of the dielectric constants of the particle and non-polar fluid.

If the electric field is created by charges at the *particle/water* interface (figure 3c), the effective dipole moment p_d can be estimated from the expression [26,27,29,30]

$$p_d = \frac{4\pi\varepsilon_n\sigma_{pw}R_p^2(1 + \cos \theta)}{\varepsilon_w\kappa}, \quad (3.3)$$

where ε_w is the dielectric constant of water and σ_{pw} is the electric charge density at the particle/water interface. Because $\kappa \propto I^{1/2}$ (I is the ionic strength in the water) the dipole moment p_d given by equation (3.3) decreases upon the addition of electrolyte in the aqueous phase, whereas p_d given by equation (3.2) should be insensitive to the concentration of electrolyte in the water. This was observed with 1 μm silica particles at the octane/water interface: electrolyte concentrations up to 1 M NaCl in the water phase did not alter the interparticle distances [31].

(b) Model of surface pressure with a pairwise additive interparticle force

The first model of the electrostatic surface pressure, Π_{el} , acting in a monolayer of charged particles at a water/non-polar fluid interface was proposed by Aveyard *et al.* [4]. The particles were modelled as finite dipoles consisting of two opposite charges (original charge and image

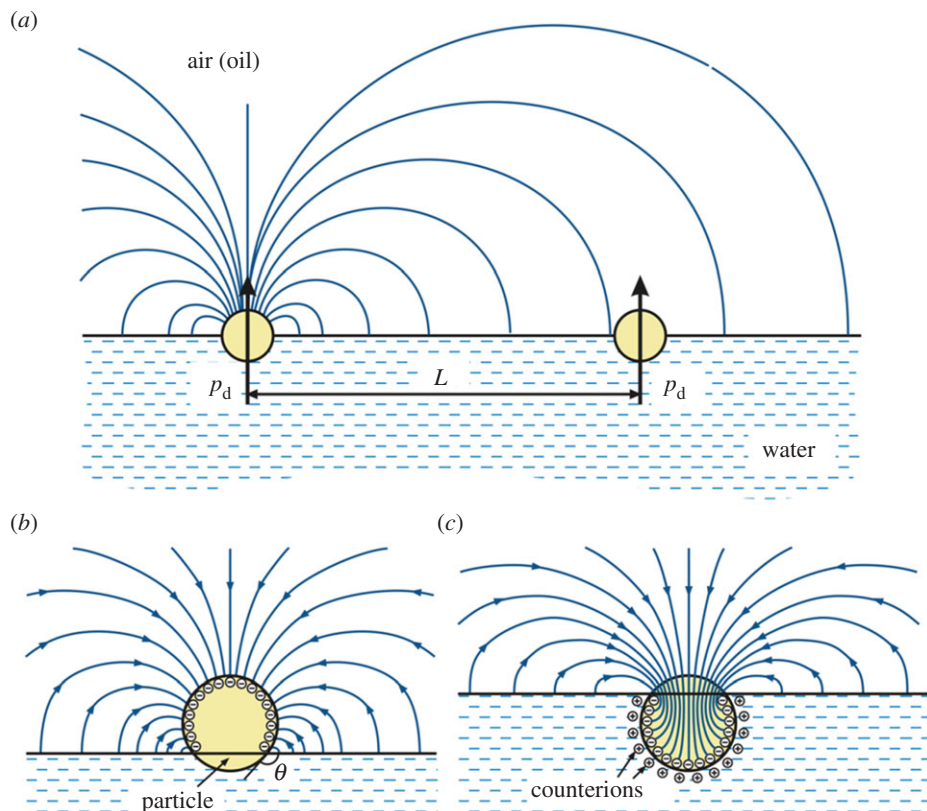


Figure 3. (a) Two charged particles at the interface between water and a non-polar fluid (air or oil): the electric field of each particle in the non-polar fluid is asymptotically equivalent to the field of a dipole of dipole moment p_d (equation (3.1)); L is the centre-to-centre distance between the particles. The electric field in the non-polar fluid can be created by charges located (b) at the particle/non-polar fluid interface and (c) at the particle/water interface; θ is the three-phase contact angle of the particle at the liquid interface. (Online version in colour.)

Table 1. Values of $Z_1 n^{1/4}$ and n determined from the experimental curves.

	$Z_1 n^{1/4}$ from the slope	aggregation number, n
<i>experiment 1</i>		
water, cycle 1	1.58×10^5	1
water, cycle 2	1.72×10^5	1.39
water, cycle 3	1.85×10^5	1.89
water, cycle 4	1.94×10^5	2.29
<i>experiment 2</i>		
water, cycle 1	1.09×10^5	1.00
0.1 mM KCl ^a	1.51×10^5	3.47 ^b
1.0 mM KCl ^a	2.00×10^5	10.8 ^b

^aThe parameter values for KCl solutions are averaged over three cycles.

^bLower limit of n estimated assuming $Z_1 = 1.09 \times 10^5$ as for experiment 2, water, cycle 1.

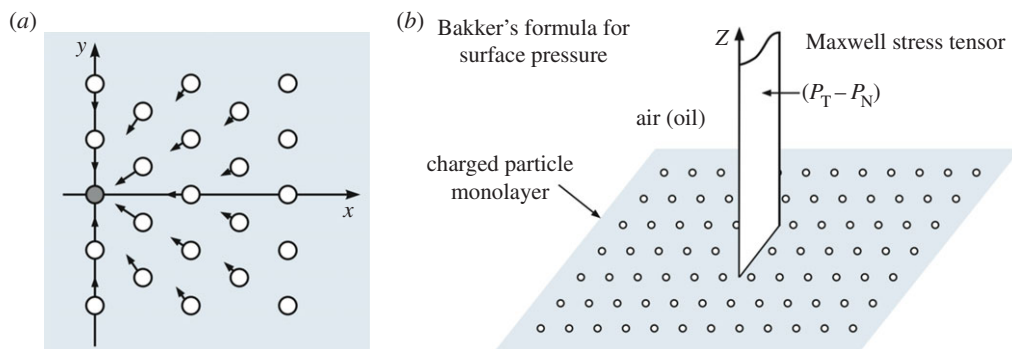


Figure 4. Expressions for the surface pressure due to the electrostatic repulsion between the charged particles in the monolayer can be derived (a) by summing up the forces of interaction of a given particle with all other particles in the half-space $x > 0$ assuming pairwise additivity [4] and (b) by integrating the Maxwell stress tensor of the electric field produced by the particles in the monolayer in accordance with the Bakker formula [23]. (Online version in colour.)

charge) of magnitude q separated at a distance 2ζ . In such a case, the force of electrostatic repulsion between two particles, F_{ER} , obeys equation (3.1) with $p_d = 2\zeta q$. Furthermore, Π_{el} has been calculated by summing up the interaction forces of a given particle with all other particles in the half-plane $x > 0$ (figure 4a). The asymptotics of the derived expression for $L \gg 2\zeta$ is [4]

$$\Pi_{el} = \frac{3^{1/2} q^2 \zeta^2}{2\epsilon_n R_p^5 (A/A_h)^{5/2}} = 2^{3/2} 3^{7/4} \frac{q^2 \zeta^2}{\epsilon_n \alpha^{5/2}}. \quad (3.4)$$

Here, A_h is the minimal area of the monolayer at close contact between the particles; we have used the expressions $A_h = 2\sqrt{3}R_p^2 N$, which presumes hexagonal packing, and $A = N\alpha$, where α is the mean area per particle in a monolayer that contains N particles.

Equation (3.4) yields $\Pi_{el} \propto A^{-5/2} \propto L^{-5}$. By contrast, the experiment indicates that asymptotically $\Pi_{el} = \Pi - \Pi_0 \propto A^{-3/2} \propto L^{-3}$ (e.g. figure 2b,d; equation (2.1); [23]). This difference could be due to the fact that the assumption for pairwise additivity of the interparticle force (superposition approximation for particles at an interface) is not adequate in the case of the long-range dipole–dipole interaction [32]. In other words, the longer range of the experimental surface pressure, $\Pi_{el} \propto L^{-3}$, can be due to collective effects (multi-particle interactions), as demonstrated in the next subsection.

(c) Model of surface pressure taking into account multi-particle interactions

A different approach was developed in [23] to take into account multi-particle interactions. The monolayer of charged particles was modelled as a periodic lattice of surface charges (figure 4b). The electric field created by this lattice in the non-polar fluid was determined by solving the Poisson equation, along with the respective boundary condition,

$$\frac{\partial^2 \psi}{\partial x^2} + \frac{\partial^2 \psi}{\partial y^2} + \frac{\partial^2 \psi}{\partial z^2} = 0 \quad (3.5)$$

and

$$\frac{\partial \psi}{\partial z} = -\frac{4\pi}{\epsilon_n} \sigma \quad \text{at } z = 0. \quad (3.6)$$

Here, $\psi = \psi(x, y, z)$ is the electrostatic potential; x , y and z are Cartesian coordinates; the plane $z = 0$ coincides with the liquid interface; and $\sigma = \sigma(x, y)$ is the surface charge density. Zero bulk charge density has been assumed in the non-polar fluid, which leads to the zero on the right-hand

side of equation (3.5). The Maxwell pressure tensor of the electric field is [33],

$$P_{ij} = \left(p_0 + \frac{\epsilon_n}{8\pi} |\mathbf{E}|^2 \right) \delta_{ij} - \frac{\epsilon_n}{4\pi} E_i E_j, \quad \mathbf{E} \equiv -\nabla\psi, \quad (3.7)$$

where δ_{ij} ($i, j = 1, 2, 3$) is the Kronecker delta; p_0 is a background pressure; and \mathbf{E} and E_i denote the vector of the electric field and its component. The contribution of the electric field to the surface pressure, Π_{el} , can be calculated by using the Bakker formula [34]

$$\Pi_{\text{el}} = \int_0^\infty (P_T - P_N) dz, \quad (3.8)$$

where P_T and P_N are the tangential and normal components of the Maxwell pressure tensor with respect to the interface. Equation (3.8) corresponds to integration of the excess tangential pressure along a semi-infinite plate of unit width, which is situated perpendicular to the interface (figure 4b).

To simplify the calculations, it is convenient to work with a square lattice of particles with period L that corresponds to the same area per particle as the real system (of hexagonal packing). The particles can be modelled as squares of side $2R$. To calculate the macroscopic surface pressure Π_{el} , we take the average values of the acting pressures over one period of the two-dimensional lattice. For this reason, the final result is not expected to be sensitive to the shape of the elementary cell, square or hexagon of the same area. The combination of equations (3.7) and (3.8) yields [23]

$$\Pi_{\text{el}} \equiv \frac{1}{L^2} \int_{-L/2}^{L/2} dx \int_{-L/2}^{L/2} dy \int_0^\infty dz \frac{\epsilon_n}{4\pi} \left[\left(\frac{\partial\psi}{\partial z} \right)^2 - \left(\frac{\partial\psi}{\partial x} \right)^2 \right]. \quad (3.9)$$

For a square lattice of charged particles, the surface charge density, $\sigma(x, y)$, can be expanded in Fourier series,

$$\frac{\sigma}{\sigma_{\text{pn}}} = \sum_{m=1}^\infty a_{m,0} \cos\left(m\pi \frac{2x}{L}\right) + \sum_{n=1}^\infty a_{0,n} \cos\left(n\pi \frac{2y}{L}\right) + \sum_{m,n=1}^\infty a_{m,n} \cos\left(m\pi \frac{2x}{L}\right) \cos\left(n\pi \frac{2y}{L}\right). \quad (3.10)$$

Here, σ is scaled with the charge density at the particle/non-polar fluid interface, σ_{pn} ; $a_{m,n}$ ($m, n = 0, 1, 2, \dots$) are dimensionless coefficients, which can be determined if the function $\sigma(x, y)$ is specified. Equation (3.10) is applicable also to the case when the electric field in the non-polar fluid is created by charges of surface density σ_{pw} located at the particle/water interface (figure 3c). In the latter case, σ_{pn} in equation (3.10) should be formally expressed in terms of σ_{pw} using eqns (27) and (29) in [23].

Solving the boundary problem consisting of equations (3.5), (3.6) and (3.10), and substituting the obtained $\psi(x, y, z)$ in equation (3.9), one obtains

$$\Pi_{\text{el}} = \frac{\sigma_{\text{pn}}^2 L}{2\epsilon_n} \left(\sum_{m=1}^\infty \frac{a_{0,m}^2}{m} + \frac{1}{2} \sum_{m,n=1}^\infty \frac{m^2 a_{m,n}^2}{(m^2 + n^2)^{3/2}} \right). \quad (3.11)$$

Equation (3.11) expresses the electrostatic surface pressure for any periodic distribution of the surface charges, $\sigma(x, y)$, described by equation (3.10). In [23], the function $\sigma(x, y)$ has been specified for a cell model of surface charge density distribution and the coefficients $a_{m,n}$ have been determined. The summation in equation (3.11) has led to the following expression for the electrostatic component of surface pressure:

$$\Pi_{\text{el}} = \frac{\sigma_{\text{pn}}^2 R}{\epsilon_n} F(\xi), \quad \xi \equiv \frac{2R}{L} = \left(\frac{\alpha}{\alpha_h} \right)^{-1/2}. \quad (3.12)$$

Here, $2R$ is the value of L at close contact between two particles; as before, α is the area per particle in the monolayer; α_h is the minimal possible value of α at close contact; ξ is a dimensionless parameter; $F(\xi) \equiv F(\xi, 20)$ is a universal dimensionless function, which is obtained analytically in the form of series expansion and tabulated (see table S1 in the Supporting Information appended to [23]). In figure 5a, F is plotted versus $\xi^3 = (\alpha/\alpha_h)^{-3/2}$; this shows that for $\xi^3 \leq 0.4$ the plot

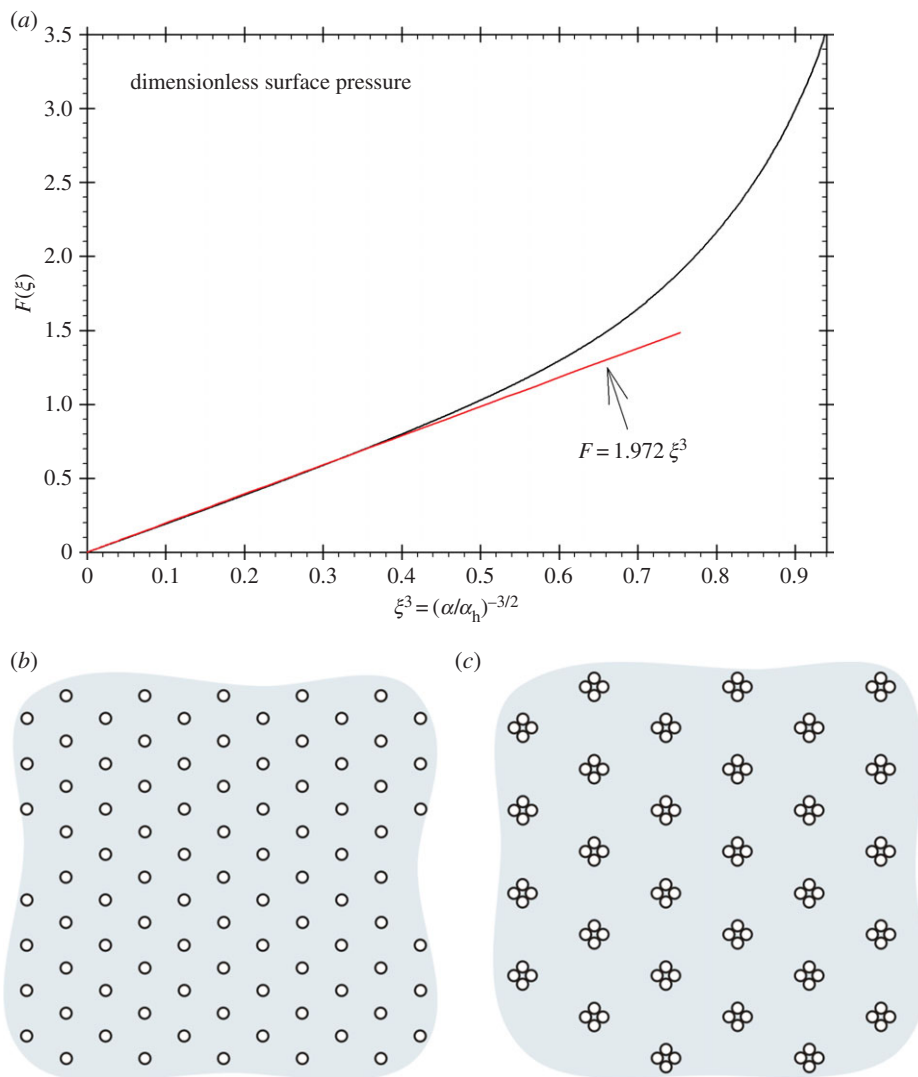


Figure 5. (a) The plot of the theoretical dimensionless electrostatic surface pressure, F , versus $\xi^3 = (\alpha/\alpha_h)^{-3/2}$ can be accurately approximated with a straight line, $F = 1.972\xi^3$, for $\xi^3 < 0.4$. (b) Sketch of an interfacial monolayer that consists of single particles; (c) sketch of a monolayer that consists of the same particles but in the form of aggregates of n particles ($n = 4$). (Online version in colour.)

complies with a linear dependence, in agreement with the behaviour of the experimental data in figure 2*b,d* (we recall that $A = N\alpha$, where $N = \text{const.}$). Hence, the function $F(\xi)$ can be estimated from the *asymptotic* formula (figure 5*a*) [24]

$$F \approx 1.972 \left(\frac{\alpha}{\alpha_h} \right)^{-3/2} \quad \text{for} \quad \left(\frac{\alpha}{\alpha_h} \right)^{-3/2} \leq 0.4. \quad (3.13)$$

The simple form of equation (3.13) makes the quantitative interpretation of surface-pressure isotherms much easier. Combining equations (2.1), (3.12) and (3.13), one can express the total surface pressure in the form

$$\Pi = 1.972 \frac{\sigma_{pn}^2 R}{\varepsilon_n} \left(\frac{\alpha}{\alpha_h} \right)^{-3/2} + \Pi_0. \quad (3.14)$$

For the square-lattice model used in this study, we have $\alpha_n = (2R)^2$ and $Ze = (2R)^2|\sigma_{pn}|$, where e is the elementary electric charge and Z is the average number of elementary charges per particle. Thus, equation (3.14) acquires the form [24]

$$\Pi = 0.986 \frac{(Ze)^2}{\varepsilon_n \alpha^{3/2}} + \Pi_0. \quad (3.15)$$

The parameters R and σ_{pn} of the auxiliary square-lattice model do not take part in equation (3.15). Indeed, as already mentioned, the asymptotic expression for Π is not expected to be sensitive to the use of a square or hexagonal lattice (with the same α and Z) because Π is a macroscopic quantity that is obtained by averaging over the interface (equation (3.9)).

(d) Surface pressure of a monolayer from weakly aggregated charged particles

Let us compare the surface pressure of a monolayer of single charged particles (figure 5*b*) with that of a monolayer which consists of the same particles, but in the form of aggregates of n particles (figure 5*c*). The number of aggregates is $N_a = N/n$, where N is the total number of particles in the monolayer. If we consider the aggregates in figure 5*c* as bigger particles, their charge and area per particle are

$$Z = nZ_1, \quad \alpha = \frac{A}{N_a} = \frac{nA}{N}, \quad (3.16)$$

where Z_1 is the number of charges per single particle. Substitution of Z and α from equation (3.16) in equation (3.15) yields [24]

$$\Pi = 0.986 \frac{(Z_1 e)^2 N^{3/2}}{\varepsilon_n} \frac{n^{1/2}}{A^{3/2}} + \Pi_0. \quad (3.17)$$

Equation (3.17) predicts that the electrostatic component of the surface pressure, $\Pi_{el} = \Pi - \Pi_0$, should increase proportional to $n^{1/2}$, i.e. the surface pressure of a monolayer of charged particles should increase with particle aggregation. This result can explain the increase in the slope of the experimental plots in figure 2*c,d* with the increase in n with aggregation.

The values of N obtained from the slope of the plot of α (determined from photographs) versus A are known; in our case, they are [24]

$$N = 21.7 \times 10^6 \text{ (experiment 1)} \quad \text{and} \quad N = 28.7 \times 10^6 \text{ (experiment 2)}. \quad (3.18)$$

In our experiments, the greatest compression of the monolayer was at a minimal surface area of $A = 14.4 \text{ cm}^2$, which in view of equation (3.18) corresponds to a mean area per particle $\alpha = A/N = 66.4 \text{ }\mu\text{m}^2$ (experiment 1) and $\alpha = 50.3 \text{ }\mu\text{m}^2$ (experiment 2). For comparison, the smallest area per particle at close contact is $\alpha_h = 2\sqrt{3}R_p^2 = 12.8 \text{ }\mu\text{m}^2$. The fact that aggregation is observed at not too high a degree of compression (the minimal experimental α is considerably greater than α_h) is an indication of the action of long-range interparticle attraction, as discussed in §4*c*.

From the slopes of the Π versus $A^{-3/2}$ plots in figure 2*b*, using equations (3.17) and (3.18) we can calculate the product $Z_1 n^{1/4}$ (table 1). The observations made using the microscope of the particle monolayers indicate that in cycle 1 on the surface of the water the particle aggregation is negligible, i.e. $n = 1$. Then, in view of table 1 we obtain

$$Z_1 = 1.58 \times 10^5 \text{ (experiment 1)} \quad \text{and} \quad Z_1 = 1.09 \times 10^5 \text{ (experiment 2)}. \quad (3.19)$$

From the values of Z_1 in equation (3.19), we can estimate the surface electric charge density (σ) under the assumption that the charges that create the electric field are located on the particle/air

interface (figure 3b); arguments in favour of this assumption are discussed below. Geometrical considerations yield the following relation between σ and Z_1 :

$$2\pi R_p^2(1 - \cos\theta)\sigma = Z_1e. \quad (3.20)$$

Our particles have mean radius $R_p = 1.92 \mu\text{m}$ and the contact angle is $\theta = 94^\circ$. Then, from equations (3.19) and (3.20), we estimate

$$\sigma = 0.102 \mu\text{C cm}^{-2} \text{ (experiment 1)} \quad \text{and} \quad \sigma = 0.071 \mu\text{C cm}^{-2} \text{ (experiment 2)}. \quad (3.21)$$

The above two values correspond to an area per surface charge of 157 and 227 nm², respectively. The values of σ in equation (3.21) are of the same order of magnitude as those determined in [23].

Furthermore, assuming that Z_1 remains the same in the subsequent compression/expansion cycles of experiment 1 (cycles 2, 3 and 4), one can explain the increase in the slopes of the respective surface-pressure isotherms in figure 2b by an increase in the value of the mean aggregation number n . The values of n determined in this way are shown in figure 2b and are listed in table 1. The results indicate that, during experiment 1, the aggregation happens in the most compressed state of the monolayer, in which it rests for 100 s in each cycle.

Likewise, one can explain the increase in the slope of the experimental plots in the presence of KCl (experiment 2, figure 2d and table 1) by the particle aggregation engendered by the electrolyte. Assuming that the particle charge Z_1 is the same in the presence of the electrolyte, from the data in table 1 we estimate that $n = 3.47$ and 10.8, respectively, for 0.1 and 1.0 mM KCl in the water phase. However, in this case it is more reasonable to expect that the values of Z_1 in the presence of KCl are somewhat lower than those on the surface of water (which enhances the aggregation), so that the real values of n could be even greater (see the discussion in §4b).

4. Discussion

(a) Criterion for determining the location of the surface charges that create the electric field

The criterion that enables one to determine whether the electrostatic repulsion between colloid particles at a liquid interface is due to electric charges located at the particle/non-polar fluid interface (figure 3b) or at the particle/water interface (figure 3c) can be formulated in the following way. Let us consider charges of surface density σ_{pw} located at the particle/water interface. The relation between σ_{pw} and the respective particle surface electric potential, φ_s , is given by the Gouy (Graham) equation [35,36],

$$\frac{\sigma_{\text{pw}}}{e} = \frac{4I}{\kappa} \sinh\left(\frac{\Phi_s}{2}\right), \quad \Phi_s \equiv \frac{e|\varphi_s|}{kT}, \quad (4.1)$$

where I is the ionic strength of the aqueous solution and Φ_s is the dimensionless electric potential of the particle/water interface. Equation (4.1) is valid for thin electric double layers, $\kappa R_p \gg 1$, which is usually fulfilled for micrometre-sized particles. Eliminating p_d between equations (3.2) and (3.3), and substituting σ_{pw} from equation (4.1), we obtain [24]

$$\sigma = \frac{\varepsilon_n(1 + \cos\theta)e}{2\pi\varepsilon_w L_B R_p D \sin^3\theta} \sinh\left(\frac{\Phi_s}{2}\right). \quad (4.2)$$

The expression $\kappa^2 = 8\pi L_B I$ has been used, where $L_B = e^2/(\varepsilon_w kT)$ is the Bjerrum length; $L_B = 0.72 \text{ nm}$ for water at 25°C. It is remarkable that the coefficient before the hyperbolic sine in equation (4.2) does not contain the solution's ionic strength, I . Equation (4.2) means that the electric potential Φ_s at the particle/water interface creates the *same* electrostatic interparticle repulsion as charges of surface density σ at the particle/*non-polar fluid* interface.

The criterion based on equation (4.2) works as follows. (i) Φ_s is approximately set equal to the electrophoretically measured ζ -potential and then σ is calculated from equation (4.2). (ii) The value of σ is independently determined from the slope of the experimental Π versus $A^{-3/2}$ plot (e.g. figure 2b; equation (3.21)). If the values of σ determined in the two different ways are close to each other, this would mean that the interparticle repulsion is due to charges at the particle/water

interface. By contrast, if the value of σ determined from Φ_s is considerably smaller than that obtained from the slope of the Π versus $A^{-3/2}$ plot, then the interparticle repulsion is due to charges at the particle/non-polar fluid interface.

The measured ζ -potential of our hydrophobized silica particles is -57 mV (at $I = 0.1$ mM), which corresponds to $\Phi_s = 2.22$. The other parameter values are $R_p = 1.92$ μm ; $\theta = 94^\circ$; $\varepsilon_w = 78.2$; $\varepsilon_p = 4$; $\varepsilon_n = 1$; and $D \approx 0.3135$ [28]. Substituting these values in equation (4.2), we calculate $\sigma = 0.954 \times 10^{-4}$ $\mu\text{C cm}^{-2}$. The value obtained is much smaller than σ in equation (3.21), which means that the interparticle repulsion is due to charges at the particle/non-polar fluid interface.

Because of the presence of R_p in the denominator of equation (4.2), the contribution of charges located at the particle/water interface is expected to be greater for smaller particles.

(b) Possible origin of the surface charges at the particle/non-polar fluid interface

This issue has already been the subject of discussions in the literature [17,37]. A possible reason for such surface charges is the adsorption of ions from the air on the particles during their contact with the atmosphere. The adsorbing ions are most probably H^+ and/or OH^- , which are due to dissociated H_2O molecules in the water vapour [38–40]. For example, atmospheric air contains 200–800 negative ions per cubic centimetre under normal fair weather conditions [41].

The silica particles have a higher dielectric constant ($\varepsilon_p = 3.9$) than the non-polar fluid (air, $\varepsilon_n = 1$), and for this reason they attract charges dispersed in the atmospheric air because of the electrostatic image force (e.g. [33]). Depending on whether the solid is acidic or basic, the preferential adsorption of OH^- or H^+ ions on the solid/air interface leads to negative or positive surface potentials, respectively [40]. In contact with humid air, water is chemisorbed at the silica surface, forming a silanol (Si-OH) layer covered with an adsorption bilayer of H-bonded water molecules [42,43]. In this layer, OH^- ions could also bind, because they form stronger H-bonds than the H_2O molecules. This can explain the negative charge at the silica-particle/air interface in our experiments.

The hydrophobization by DCDMS consists in replacing Si-OH groups by $(\text{SiO})_2\text{-Si-(CH}_3)_2$ groups [44,45]. It has been found that not all surface silanol groups interact with the hydrophobizing agent; for example, only a small fraction of the mutually H-bonded OH groups react with the silanizing agent [46]. In our case, a value of $\theta = 94^\circ$ for the contact angle indicates a relatively low degree of hydrophobization. We could hypothesize that a considerable fraction of the hydrophobized particle/air interface is covered by silanol groups with an adjacent adsorption bilayer of water molecules and OH^- ions, whereas the silanized groups cover the rest of the interface. In other words, we could expect that at $\theta = 94^\circ$ the interface represents a two-dimensional dispersion of hydrophilic and hydrophobic surface patches. The binding of OH^- to the hydrophilic patches should be strong enough to preserve the negative surface charge when the particles are stored in IPA for more than one week, as experimentally observed.

A possible reason for the enhancement of aggregation with the increase in KCl concentration could be the migration of K^+ ions from the aqueous phase to the particle/air interface, which leads to a decrease in the net negative particle charge, Z . Indeed, the subsurface layer of the particle/water interface is enriched in K^+ counterions (figure 3c), from where they could move towards the particle/air interface, attracted by its negative charge. The medium that favours such migration could be the fraction of the particle/air interface that is covered by hydrophilic patches (silanol groups) with an adjacent adsorption bilayer of water molecules and OH^- ions [42,43]. Migration of OH^- ions along the silica/air interface under the action of the tangential electric potential difference has already been detected [38]. The surface conductivity of SiO_2 has been found to decrease upon silanization [44], which also leads to a decrease in the silica-particle surface charge, as observed in our experiments.

In [31], the electrolyte concentration was increased to 1 M NaCl without suppressing the electrostatic interparticle forces. However, in these experiments the non-polar fluid was octane (rather than humid air), which might have blocked any migration of hydrophilic Na^+ counterions towards the particle/oil interface.

(c) Origin of the attractive force that causes the aggregation of charged particles

To have particle aggregation, an attractive force that can overcome the powerful electrostatic repulsion (see equation (3.1)) is needed. The gravity-induced capillary attraction between floating particles [47,48] cannot be the reason for aggregation, because the weight of our particles is too small. In [17], it was proposed that the reason for aggregation could be the attractive force between capillary quadrupoles, F_q , which is due to out-of-plane undulations of the contact lines on particle surfaces [49–52]. These undulations are related to the hysteresis of the three-phase contact angle, which is present as a rule at solid surfaces (even at smooth ones)—its absence being exclusion [53–56]. In our case, the reason for hysteresis could be the inhomogeneous wettability of the particle surface, which most probably represents a two-dimensional dispersion from hydrophilic and hydrophobic patches at $\theta = 94^\circ$ (see above).

Because $F_q \propto L^{-5}$, this capillary force could overcome the electrostatic repulsion ($F_{ER} \propto L^{-4}$) at short distances. The distance at which the total force is zero corresponds to the position of the energy barrier to particle aggregation. Substituting the expressions for F_{ER} from equations (3.1) and (3.2), and F_q from [49,50], in the equation $F_{ER} + F_q = 0$, we obtain

$$\frac{3(2DZ_1eR_p \sin^3 \theta)^2}{2\varepsilon_n L^4 (1 - \cos \theta)^2} - 48\pi \gamma H^2 \frac{r_c^4}{L^5} = 0. \quad (4.3)$$

Here, γ is the surface tension of the liquid interface; H is the amplitude of the contact-line undulations; and $r_c = R_p \sin \theta$ is the mean radius of the three-phase contact line on the particle surface. (The cosine in the formula for F_q has been set equal to 1, which corresponds to the energetically most favourable configuration of the two capillary quadrupoles.) Substituting typical parameter values— $R_p = r_c = 2 \mu\text{m}$, $L = 3R_p = 6 \mu\text{m}$; $\gamma = 72 \text{ mN m}^{-1}$; $e = 4.80 \times 10^{-10}$ statcoulombs; $Z_1 = 10^{-5}$ (table 1), $\theta = 90^\circ$; $\varepsilon_p = 4$, $\varepsilon_n = 1$ and $D = 0.3135$ [28]—from equation (4.3) we calculate $H = 0.433 \mu\text{m}$, which is a reasonable value for the amplitude of contact-line undulations on the surface of a particle of diameter $\approx 4 \mu\text{m}$. Hence, the aggregation of charged particles in these experiments can really be due to attraction between capillary quadrupoles [24].

(d) Concept for limited aggregation of charged particles at a liquid interface

In view of equation (3.17), the presence of long linear portions in the Π versus $A^{-3/2}$ plots in figure 2*b,d* indicates that the average aggregation number, n , has been constant during the respective compression or expansion of the particle monolayer. This result leads to the concept of *limited aggregation* of particles [24], which is logically analogous to the limited coalescence in Pickering emulsions [57–59]. Indeed, the particle aggregation enhances the electrostatic repulsion between the aggregates and the monolayer's surface pressure ($\Pi_{el} \propto n^{1/2}$). This leads to a rise in the electrostatic barrier to aggregation and, eventually, to the cessation of aggregation, i.e. we are dealing with negative feedback. In addition, particle aggregates with $n \geq 3$ should behave as capillary multipoles of higher order that experience capillary attraction of shorter range [51,52], which means weaker attraction and a higher barrier to coalescence upon aggregation.

As already mentioned, the increase in Π with the number of compression/expansion cycles in the case of experiment 1 (figure 2*b*) could be explained by overcoming the barrier only in the most compressed state of the monolayer, i.e. during the interval of 100 s after the end of compression and before the start of the subsequent expansion. In such a case, the process of limited aggregation would happen in a *stepwise* manner, as experimentally observed (figure 2*b*).

If the particles have a lower surface charge, the barrier to aggregation would be lower and the limited coalescence would be expected to occur faster. This seems to be the case with our experiment 2, where the isotherms obtained upon compression (or upon expansion) are very reproducible (figure 2*d*). This indicates *complete* limited coalescence. The hysteresis (the difference between the experimental curves obtained upon compression and expansion; figure 2*d*) could be

explained by the presence of loosely connected aggregates that coalesce upon compression, but split upon expansion.

5. Conclusion

Recent results [23,24] reviewed in the present article indicate that the surface pressure, Π , of a monolayer of charged colloid particles at a liquid interface is dominated by collective effects (multi-particle interactions) that lead to a relatively long-range asymptotics, $\Pi \propto L^{-3}$, at large interparticle separations, L (equation (3.15)). Particle aggregation in such monolayers has also been observed. For a higher particle charge, the aggregation may happen only in the monolayer's most compressed state. For a lower particle charge, and especially in the presence of electrolyte in the aqueous phase, the aggregation may happen spontaneously. An attractive force that can overcome the long-range dipole–dipole repulsion between the particles and cause aggregation is the attraction between capillary quadrupoles due to an undulated contact line on particle surfaces [17].

The charge on the surface aggregates is greater than that on the separate particles. However, the distances between the aggregates are also greater than those between the dispersed particles (figure 5*b,c*). The combination of these two effects leads to an increase of the electrostatic surface pressure with aggregation number, $\Pi_{\text{el}} \propto n^{1/2}$. This result can explain the observed increase of Π upon consecutive compression/expansion cycles, as well as upon addition of electrolyte in the aqueous subphase. The increase in Π with the increase in n leads also to *limited aggregation*. Indeed, when the two-dimensional aggregates are sufficiently large, the barrier to aggregation becomes high enough to prevent further aggregation. This circumstance can explain the very reproducible Π versus A isotherms of monolayers from weakly or moderately aggregated particles.

A criterion for establishing the location of the charges that create the electrostatic repulsion between particles in the investigated monolayers has been proposed (equation (4.2)). Its application to the system studied in [23,24] indicates that the source of the electrostatic repulsion is the charges at the particle/air (rather than at the particle/water) interface. The negative charges at the silica/air interface could be due to adsorption of OH^- ions from the humid atmospheric air on the acidic SiO_2 interface [40]. The suppression of the charge at the particle/air interface by added electrolyte (KCl) in the aqueous phase could be explained by the migration of K^+ counterions to the negatively charged upper particle surface, facilitated by water molecules condensed on this surface from the air [42,43]. The experiment [31] indicates that, if the upper fluid phase is oil (instead of air), such migration is impossible.

The results presented and discussed in this article could contribute to a deeper understanding of the interactions in monolayers of charged particles at liquid interfaces. A challenge for future investigations is the computer simulation of aggregation and phase transitions in such monolayers, which could essentially complement the analytical theory presented here. So far, simulations of two-dimensional particle arrays with repulsive long-range interactions have been carried out in the case of the Yukawa potential, which decays exponentially with the interparticle distance, L [60–62]. In the systems considered here, the long-range interparticle forces, $F_{\text{ER}} \propto 1/L^4$ and $F_{\text{q}} \propto -1/L^5$, may lead to interesting and unexpected new results, such as the (apparently) paradoxical increase in electrostatic surface pressure upon the addition of electrolyte to the water phase [24].

Authors' contributions. P.A.K. conceived and coordinated the work, participated in data analysis and interpretation, and drafted the manuscript; K.D.D. developed the theoretical model, carried out mathematical derivations and numerical computations, and compared theory and experiment; P.V.P. carried out all experiments, including particle hydrophobization, surface pressure and ζ -potential measurements, microscopic observations and video recordings, and performed primary statistical analysis of the obtained results. All authors gave final approval for publication.

Competing interests. The authors declare that they have no competing interests.

Funding. The authors gratefully acknowledge support from the National Science Fund of Bulgaria, grant no. DO-02-121/2009, and from COST Action CM1101.

References

- Schuller H. 1967 Modellversuche zur Spreitung von Kolloid-Partikeln. *Kolloid Z. Z. Polym.* **216**, 380–383. (doi:10.1007/BF01525107)
- Sheppard E, Tcheurekdjian N. 1968 Monolayer studies. IV. Surface films of emulsion latex particles. *J. Colloid Interface Sci.* **28**, 481–486. (doi:10.1016/0021-9797(68)90080-5)
- Pieranski P. 1980 Two-dimensional interfacial colloidal crystals. *Phys. Rev. Lett.* **45**, 569–572. (doi:10.1103/PhysRevLett.45.569)
- Aveyard R, Clint JH, Nees D, Paunov VN. 2000 Compression and structure of monolayers of charged latex particles at air/water and octane/water interfaces. *Langmuir* **16**, 1969–1979. (doi:10.1021/la990887g)
- Reynaert S, Moldenaers P, Vermant J. 2006 Control over colloidal aggregation in monolayers of latex particles at the oil-water interface. *Langmuir* **22**, 4936–4945. (doi:10.1021/la060052n)
- Aveyard R *et al.* 2002 Measurement of long-range repulsive forces between charged particles at an oil-water interface. *Phys. Rev. Lett.* **88**, 246102. (doi:10.1103/PhysRevLett.88.246102)
- Zhao Y, Wang J, Mao G. 2005 Colloidal subwavelength nanostructures for antireflection optical coatings. *Opt. Lett.* **30**, 1885–1887. (doi:10.1364/OL.30.001885)
- Ray MA, Jia L. 2007 Micropatterning by non-densely packed interfacial colloidal crystals. *Adv. Mater.* **19**, 2020–2022. (doi:10.1002/adma.200602521)
- Min W-L, Jiang P, Jiang B. 2008 Large-scale assembly of colloidal nanoparticles and fabrication of periodic subwavelength structures. *Nanotechnology* **19**, 475604. (doi:10.1088/0957-4484/19/47/475604)
- Cayre OJ, Paunov VN. 2004 Fabrication of microlens arrays by gel trapping of self-assembled particle monolayers at the decane–water interface. *J. Mater. Chem.* **14**, 3300–3302. (doi:10.1039/B413361G)
- Sun Y, Forrest SR. 2006 Organic light emitting devices with enhanced outcoupling via microlenses fabricated by imprint lithography. *J. Appl. Phys.* **100**, 073106. (doi:10.1063/1.2356904)
- Isa L, Kumar K, Müller M, Grolig J, Textor M, Reimhult E. 2010 Particle lithography from colloidal self-assembly at liquid–liquid interfaces. *ACS Nano* **4**, 5665–5670. (doi:10.1021/nn101260f)
- Bettinger CJ, Langer R, Borenstein JT. 2009 Engineering substrate micro- and nanotopography to control cell function. *Angew. Chem. Int. Ed.* **48**, 5406–5415. (doi:10.1002/anie.200805179)
- Crossley S, Faria J, Shen M, Resasco DE. 2010 Solid nanoparticles that catalyze biofuel upgrade reactions at the water/oil interface. *Science* **327**, 68–72. (doi:10.1126/science.1180769)
- Garbin V, Crocker JC, Stebe KJ. 2012 Nanoparticles at fluid interfaces: exploiting capping ligands to control adsorption, stability and dynamics. *J. Colloid Interface Sci.* **387**, 1–11. (doi:10.1016/j.jcis.2012.07.047)
- Stancik EJ, Kouhkan M, Fuller GG. 2004 Coalescence of particle-laden fluid interfaces. *Langmuir* **20**, 90–94. (doi:10.1021/la0356093)
- Horozov TS, Binks BP. 2005 Particle behavior at horizontal and vertical fluid interfaces. *Colloids Surf. A* **267**, 64–73. (doi:10.1016/j.colsurfa.2005.06.037)
- Horozov TS, Aveyard R, Clint JH, Neumann B. 2005 Particle zips: vertical emulsion films with particle monolayers at their surfaces. *Langmuir* **21**, 2330–2341. (doi:10.1021/la047993p)
- Xu H, Kirkwood J, Lask M, Fuller G. 2010 Charge interaction between particle-laden fluid interfaces. *Langmuir* **26**, 3160–3164. (doi:10.1021/la903099a)
- Jarpa-Parra M, Bamdad F, Tian Z, Zeng HB, Temelli F, Chen L. 2015 Impact of pH on molecular structure and surface properties of lentil legumin-like protein and its application as foam stabilizer. *Colloids Surf. B* **132**, 45–53. (doi:10.1016/j.colsurfb.2015.04.065)
- Bykov AG, Loglio G, Miller R, Noskov BA. 2015 Dilational surface elasticity of monolayers of charged polystyrene nano- and microparticles at liquid/fluid interfaces. *Colloids Surf. A* **485**, 42–48. (doi:10.1016/j.colsurfa.2015.09.004)
- Danov KD, Kralchevsky PA, Ananthapadmanabhan KP, Lips A. 2006 Interpretation of surface-tension isotherms of *n*-alkanoic (fatty) acids by means of the van der Waals model. *J. Colloid Interface Sci.* **300**, 809–813. (doi:10.1016/j.jcis.2006.04.026)

23. Petkov PV, Danov KD, Kralchevsky PA. 2014 Surface pressure isotherm for a monolayer of charged colloidal particles at a water/nonpolar-fluid interface: experiment and theoretical model. *Langmuir* **30**, 2768–2778. (doi:10.1021/la500126d)
24. Petkov PV, Danov KD, Kralchevsky PA. 2016 Monolayers of charged particles in a Langmuir trough: could particle aggregation increase the surface pressure? *J. Colloid Interface Sci.* **462**, 223–234. (doi:10.1016/j.jcis.2015.09.075)
25. Danov KD, Kralchevsky PA. 2013 Forces acting on dielectric colloidal spheres at a water/nonpolar-fluid interface in an external electric field. 2. Charged particles. *J. Colloid Interface Sci.* **405**, 269–277. (doi:10.1016/j.jcis.2013.05.015)
26. Hurd AJ. 1985 The electrostatic interaction between interfacial colloidal particles. *J. Phys. A* **18**, L1055–L1060. (doi:10.1088/0305-4470/18/16/011)
27. Paunov VN. 2003 Electrostatic interaction between charged colloid particles entrapped in a thin electrolyte film: confinement effects. *Colloid Polym. Sci.* **281**, 701–707. (doi:10.1007/s00396-002-0820-y)
28. Danov KD, Kralchevsky PA. 2006 Electric forces induced by a charged colloid particle attached to the water–nonpolar fluid interface. *J. Colloid Interface Sci.* **298**, 213–231. (doi:10.1016/j.jcis.2005.12.037)
29. Oettel M, Dietrich S. 2008 Colloidal interactions at fluid interfaces. *Langmuir* **24**, 1425–1441. (doi:10.1021/la702794d)
30. Park BJ, Pantina JP, Furst EM, Oettel M, Reynaert S, Vermant J. 2008 Direct measurements of the effects of salt and surfactant on interaction forces between colloidal particles at water–oil interfaces. *Langmuir* **24**, 1686–1694. (doi:10.1021/la7008804)
31. Horozov TS, Aveyard R, Clint JH, Binks BP. 2003 Order–disorder transition in monolayers of modified monodisperse silica particles at the octane–water interface. *Langmuir* **19**, 2822–2829. (doi:10.1021/la020858x)
32. Majee A, Markus Bier M, Dietrich S. 2014 Electrostatic interaction between colloidal particles trapped at an electrolyte interface. *J. Chem. Phys.* **140**, 164906. (doi:10.1063/1.4872240)
33. Landau LD, Lifshitz EM. 1960 *Electrodynamics of continuous medium*. Oxford, UK: Pergamon Press.
34. Bakker G. 1928 Kapillarität und Oberflächenspannung. In *Handbuch der Experimentalphysik, Band 6*. Leipzig, Germany: Akademische Verlagsgesellschaft.
35. Davies JT, Rideal EK. 1963 *Interfacial phenomena*. London, UK: Academic Press.
36. Israelachvili JN. 2011 *Intermolecular and surface forces*, 3rd edn. London, UK: Academic Press.
37. Boneva MP, Danov KD, Christov NC, Kralchevsky PA. 2009 Attraction between particles at a liquid interface due to the interplay of gravity- and electric-field-induced interfacial deformations. *Langmuir* **25**, 9129–9139. (doi:10.1021/la9006873)
38. Gouveia RF, Costa CAR, Galembeck F. 2008 Water vapor adsorption effect on silica surface electrostatic patterning. *J. Phys. Chem. C* **112**, 17 193–17 199. (doi:10.1021/jp803812p)
39. Gouveia RF, Galembeck F. 2009 Electrostatic charging of hydrophilic particles due to water adsorption. *J. Am. Chem. Soc.* **131**, 11 381–11 386. (doi:10.1021/ja900704f)
40. Gouveia RF, Bernardes JS, Ducati TRD, Galembeck F. 2012 Acid–base site detection and mapping on solid surfaces by Kelvin force microscopy (KFM). *Anal. Chem.* **84**, 10 191–10 198. (doi:10.1021/ac3009753)
41. Kolarž PM, Filipović DM, Marinković BP. 2009 Daily variations of indoor air-ion and radon concentrations. *Appl. Radiat. Isot.* **67**, 2062–2067. (doi:10.1016/j.apradiso.2009.07.023)
42. Hair ML, Hertl W. 2000 Adsorption on hydroxylated silica surfaces. *J. Phys. Chem.* **73**, 4269–4276. (doi:10.1021/j100846a039)
43. Zhuravlev LT. 2000 The surface chemistry of amorphous silica. Zhuravlev model. *Colloids Surf. A* **173**, 1–38. (doi:10.1016/S0927-7757(00)00556-2)
44. Voorthuyzen JA, Keskin K, Bergveld P. 1987 Investigations of the surface conductivity of silicon dioxide and methods to reduce it. *Surf. Sci.* **187**, 201–211. (doi:10.1016/S0039-6028(87)80132-2)
45. Hair ML, Hertl W. 1969 Reactions of chlorosilanes with silica surfaces. *J. Phys. Chem.* **73**, 2372–2378. (doi:10.1021/j100727a046)
46. Hair ML, Hertl W. 1971 Reaction of hexamethyldisilazane with silica. *J. Phys. Chem.* **75**, 2181–2185. (doi:10.1021/j100683a020)
47. Chan DYC, Henry JD, White RL. 1981 The interaction of colloidal particles collected at fluid interfaces. *J. Colloid Interface Sci.* **79**, 410–418. (doi:10.1016/0021-9797(81)90092-8)

48. Paunov VN, Kralchevsky PA, Denkov ND, Nagayama K. 1992 Lateral capillary forces between floating submillimeter particles. *J. Colloid Interface Sci.* **157**, 100–112. (doi:10.1006/jcis.1993.1163)
49. Stamou D, Duschl C, Johannsmann D. 2000 Long-range attraction between colloidal spheres at the air-water interface: the consequence of an irregular meniscus. *Phys. Rev. E* **62**, 5263–5272. (doi:10.1103/PhysRevE.62.5263)
50. Kralchevsky PA, Denkov ND, Danov KD. 2001 Particles with an undulated contact line at a fluid interface: interaction between capillary quadrupoles and rheology of particulate monolayers. *Langmuir* **17**, 7694–7705. (doi:10.1021/la0109359)
51. Danov KD, Kralchevsky PA, Naydenov BN, Brenn G. 2005 Interactions between particles with an undulated contact line at a fluid interface: capillary multipoles of arbitrary order. *J. Colloid Interface Sci.* **287**, 121–134. (doi:10.1016/j.jcis.2005.01.079)
52. Danov KD, Kralchevsky PA. 2010 Capillary forces between particles at a liquid interface: general theoretical approach and interactions between capillary multipoles. *Adv. Colloid Interface Sci.* **154**, 91–103. (doi:10.1016/j.cis.2010.01.010)
53. Starov VM. 1992 Equilibrium and hysteresis contact angles. *Adv. Colloid Interface Sci.* **39**, 147–173. (doi:10.1016/0001-8686(92)80059-7)
54. Marmur A. 1994 Thermodynamic aspects of contact angle hysteresis. *Adv. Colloid Interface Sci.* **50**, 121–141. (doi:10.1016/0001-8686(94)80028-6)
55. Drelich J, Miller JD, Good RJ. 1996 The effect of drop (bubble) size on advancing and receding contact angles for heterogeneous and rough solid surfaces as observed with sessile-drop and captive-bubble techniques. *J. Colloid Interface Sci.* **179**, 37–50. (doi:10.1006/jcis.1996.0186)
56. Iliev SD. 1997 Static drops on an inclined plane: equilibrium modeling and numerical analysis. *J. Colloid Interface Sci.* **194**, 287–300. (doi:10.1006/jcis.1997.5110)
57. Whitesides TH, Ross DS. 1995 Experimental and theoretical analysis of the limited coalescence process: stepwise limited coalescence. *J. Colloid Interface Sci.* **169**, 48–59. (doi:10.1006/jcis.1995.1005)
58. Arditty S, Whitby CP, Binks BP, Schmitt V, Leal-Calderon F. 2003 Some general features of limited coalescence in solid-stabilized emulsions. *Eur. Phys. J. E* **11**, 273–281. (doi:10.1140/epje/i2003-10018-6)
59. Golemanov K, Tcholakova S, Kralchevsky PA, Ananthapadmanabhan KP, Lips A. 2006 Latex-particle-stabilized emulsions of anti-Bancroft type. *Langmuir* **22**, 4968–4977. (doi:10.1021/la0603875)
60. Cheng H, Dutta P, Elis DE, Kalia P. 1986 Molecular dynamics study of a two-dimensional system with screened Coulomb interactions. *J. Chem. Phys.* **85**, 2232–2236. (doi:10.1063/1.451118)
61. Naidoo KJ, Schnitker J. 1994 Melting of two-dimensional colloidal crystals: a simulation study of the Yukawa system. *J. Chem. Phys.* **100**, 3114–3121. (doi:10.1063/1.466453)
62. Qi W-K, Wang Z, Han Y, Chen Y. 2010 Melting in two-dimensional Yukawa systems: a Brownian dynamics simulation. *J. Chem. Phys.* **133**, 234508. (doi:10.1063/1.3506875)